Title

INVESTIGATION OF IRON OXIDE REDUCTION BY TEM PART II: MAGNETITE AND WUSTITE REDUCTION

Authors

Rau, M.-F.
Rieck, D.
Evans, J.W.

Publication Date

1985-07-01

Lawrence Berkeley Laboratory
UNIVERSITY OF CALIFORNIA

Materials & Molecular Research Division

Submitted to Reactivity of Solids

INVESTIGATION OF IRON OXIDE REDUCTION BY TEM
PART II: MAGNETITE AND WUSTITE REDUCTION

M.-F. Rau, D. Rieck, and J.W. Evans

July 1985

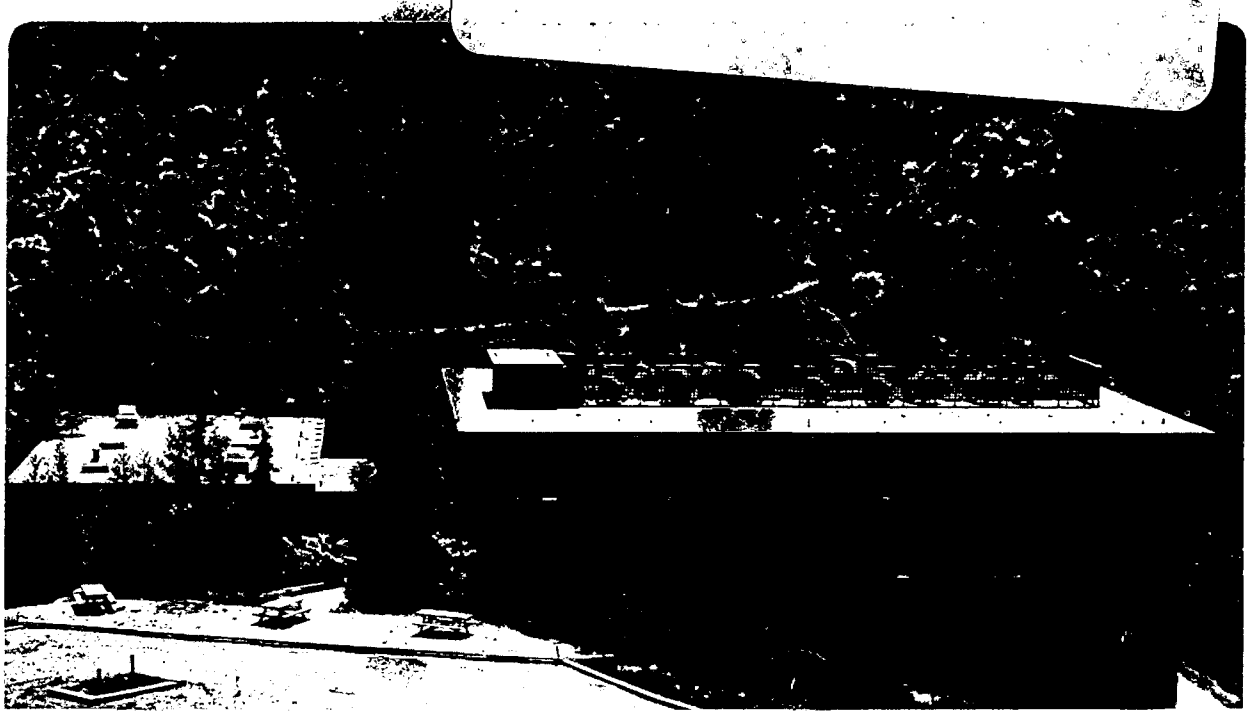

Prepared for the U.S. Department of Energy under Contract DE-AC03-76SF00098

DISCLAIMER

LBL-19961*

Investigation of Iron Oxide Reduction by TEM
Part II: Magnetite and Wustite Reduction

Mann-Fu Rau, David Rieck

and

James W. Evans†

Materials and Molecular Research Division
Lawrence Berkeley Laboratory
and
Department of Materials Science and Mineral Engineering
University of California
Berkeley, CA 94720

†Professor of Metallurgy, to whom correspondence should be addressed.

*Companion paper, LBL-19960, Investigation of Iron Oxide Reduction by TEM. Part I: Hemitite Reduction, by M.-F. Rau and J.W. Evans.

INTRODUCTION

The experimental techniques used in the investigation of magnetite and wustite reduction were identical with those described in Part I for hematite reduction. Part I also contains an account of previous investigations on these reactions.

EXPERIMENTAL RESULTS AND DISCUSSION

Magnetite reduction

Examination of the magnetite prior to reduction revealed the existence of point defects or small dislocation loops distributed on the surface; electron diffraction showed the defects to be coherent with the matrix. Figure 1 is a sequence of micrographs showing the reduction of magnetite by pure hydrogen (2 torr) at 300°C. Faceted pits appeared after approximately four minutes (see for example the left of the micrograph marked 306 seconds). Iron then nucleated in a region adjacent to the pits (left of center in micrograph at 375 s.) and the nuclei then grew across the magnetite surface. This same region before and after 13 minutes exposure to hydrogen is shown in Figure 2 at lower magnification.

Some of the nucleation sites are indicated by arrows and appear to be in the thinner regions of the specimen. Nucleation did not occur on the edge of the specimen which is in contrast to the behaviour of hematite single crystal on reduction by hydrogen (see Part I).

The faceted pits were observed to grow on exposure to hydrogen, starting with a triangular shape and then becoming six-sided. This can be seen in Figure 3 where the upper micrograph depicts 16 minutes exposure to hydrogen and the lower micrograph 17 minutes. Selective area electron diffraction

revealed that the region of the pits was still magnetite; Figure 4 shows the bright field and dark field images of a region containing a group of pits and the parallelism of some pit edges (e.g. the upper edges in this figure) should be noted. The pits are enveloped by the advancing reaction front and if they are sufficiently large or deep then they affect the morphology of the iron formed from the pitted region. This is seen in Figure 5 which is the same region as that of Figure 4 after a further 8.5 minutes exposure to hydrogen.

In the early stages of reduction the iron formed was oriented with respect to the host magnetite single crystal. This is seen in Figure 6 which is after 21 minutes exposure to 1 torr of hydrogen at 330°C. The diffraction pattern of α iron is a spot pattern rather than a ring pattern which would have occurred if non-oriented polycrystalline iron had been formed.

Figure 7 shows a region that has been partly reduced at 10 torr and 400°C. (a) is the bright field image, while (c) and (d) are the dark field images taken from rings A and B in the diffraction pattern that correspond to iron and magnetite respectively. The porous iron that is rapidly formed by this one minute exposure at this higher temperature contains considerable residual magnetite but this residual magnetite has become polycrystalline as reaction disrupts the original single crystal structure. The spotty rings appearing in the diffraction pattern are for α iron suggesting orientation of the iron in the early stages of reaction followed by disruption of this orientation as reaction proceeds.

Reduction temperature has a significant effect on the morphology of the iron formed as has been reported by others [1]. This is seen in the results

depicted in Figure 8. (a) shows the magnetite-iron interface after 10 seconds reduction with 20 torr of hydrogen at 350°C. Note the small (10-50 nm) grains of iron that have been formed at this stage. (b) is the dark field image. The sample was then brought to 500°C in vacuum and held for 2 minutes, (c) at which point the iron had pulled away from the magnetite producing the fissure running diagonally across the micrograph. (d) is the dark field image. There had been much coarsening of the iron structure. The temperature was then lowered to 300°C and the sample again exposed to hydrogen. Reaction started to the right of the fissure and proceeded slowly with the iron produced having a coarse structure. (e) shows the appearance 2 minutes after re-exposure.

The shrinkage that resulted in the fissure of Figure 8 can occur even under conditions of uninterrupted reaction and the porous iron produced by reduction of magnetite was frequently observed to be fissured, sometimes in the star-shaped pattern reported by Pluschkell and Sarma [2], see Figure 9. These large fissures in iron produced by reduction of single crystal magnetite were not found in the iron produced by reduction of hematite (Part I). A possible explanation is as follows.

The reduction of hematite proceeds with the formation of small crystals of magnetite which are then reduced to iron. The volume change on reducing magnetite to iron can readily be accommodated by shrinkage of these grains, resulting in an iron of higher porosity than the parent magnetite but without fissures. In reducing single crystal magnetite, strains due to volume change develop over the whole width of the growing iron nucleus and eventually become sufficiently large to disrupt the nucleus, forming large fissures and changing the orientation of the nucleus to the parent lattice.

When magnetite specimens were contacted with hydrogen-argon mixtures reaction proceeded very slowly (as in the case of hematite reduction). Figure 10 is a sequence of micrographs of a specimen exposed to 10% H_2/90% Ar at 350°C and 10 torr total pressure. In this instance the time on the micrographs is in minutes and, in order to achieve significant reaction in the microscope time available, iron had been nucleated by prior exposure to pure hydrogen at 10 torr, 400°C for 1 minute. The micrographs can be interpreted as showing a coarsening of the iron nucleus together with the formation of a hexagonal pit occupied by the iron phase. The walls of the pit appear to become smooth and vertical as time elapses; this is sketched in Figure 11.

Cracks and dislocation loops may play a role in the reduction. In Figure 12, which is of a specimen exposed to 10% H_2/90% Ar at 50 torr total pressure and 514°C, a crack runs horizontally across the middle of the sample. Pits have formed at this crack and elongated in a direction perpendicular to the crack. The pits appear to grow along dislocation loops (e.g. to the right of the figure). The hexagonal structures seen in Figure 13 (10% H_2/90% Ar, 10 torr, 350°C, 3 hr 12 min) may have resulted from growth of pits along dislocations. In some instances, on reducing magnetite in H_2/Ar mixtures, nucleation of the iron phase occurred at the edge of the specimen. Careful observation of the tiny (~30 nm) dislocation loops could not uncover any role that these smaller loops played in the reaction.

Wustite reduction

Wustite is thermodynamically unstable below 570°C and may be expected to disproportionate to iron and magnetite below that temperature. However the rate of disproportionation is slow so that wustite can be regarded as metastable.

Even though final thinning of the specimens was under vacuum, samples of wustite were found to contain magnetite. Electron diffraction showed the small magnetite colonies (approximately 1 μm across) to be epitaxial with the host wustite. Preliminary studies were carried out in vacuum to follow the expected thermal decomposition of the wustite to magnetite and iron. Figure 14 is a sequence of micrographs taken at 500°C; the indicated time is in minutes. The black particles on the specimen are contamination and appear to be inert. Some slight changes are observable (upper right) after a few minutes but even after 18 minutes the changes to the specimen are not large. The triangular area to the left is a growing magnetite platelet (identified by electron diffraction); presumably iron produced by the decomposition is incorporated in the host wustite by the stoichiometry range of that compound or is disseminated as areas too small to be visible. Figure 15 is a micrograph of the same area of wustite after 40 minutes at 500°C in vacuum. The minute rectangular areas are too small for identification by selected area diffraction but may be iron. When the sample was brought to 600°C the magnetite and rectangular areas were observed to slowly disappear.

The reduction of wustite by hydrogen yields iron of a structure comparable to that from magnetite reduction. Figure 16 is a sequence of micrographs of a sample exposed to 10 torr of hydrogen at 355°C. Three magnetite clusters are indicated by arrows on the micrograph of the original wustite and they were centers for nucleation of the iron, along with the edge of the specimen. The rapidity of the reduction reaction, compared to the disproportionation seen in Figure 14, should be noted. Neither an incubation period nor faceted pits were observed. Coarsening of the pores as reaction proceeds should be noted. Selected area diffraction patterns (Figure 17) from

the center of the micrograph after 2 minutes reaction showed the presence of both polycrystalline iron and magnetite. The occurrence of magnetite* in the diffraction pattern leads to the suggestion that reduction is being accompanied by disproportionation and that the latter is promoted by the former, perhaps by the iron produced by reduction. However, if iron produced by reduction promotes disproportionation then its effect must be highly localized. This is evident from an experiment in which reduction was halted after 2 minutes followed by holding the wustite sample at 400°C in vacuum for 10 minutes. No clear evidence of disproportionation could be seen during this ten minutes.

At lower pressures of reducing gas and higher temperatures, disproportionation becomes more evident. Figure 18 is a set of micrographs of a sample reduced using 0.5 torr of hydrogen at 450°C. Stereomicrographs reveal that the near rectangular structures evident in the upper two micrographs are pits bounded by raised areas (darker regions). A possible explanation in terms of disproportionation is provided in Figure 19 where the Fe_3O_4 phase (being more voluminous than FeO) protrudes above the FeO surface while the less voluminous Fe phase sinks below it. The advancing iron phase due to reduction can be seen sweeping across the specimen from the upper left in the micrograph at 485 seconds.

Disproportionation was also a dominant phenomenon in reduction of wustite with hydrogen/argon mixtures. Figure 20 shows the electron diffraction pattern on exposing wustite to 50 torr of 10% H_2/90% Ar at 514°C. (a) is the original wustite; (b) is after 14 minutes and shows the diffraction pattern of

---

*It is likely that this magnetite is not that present in the initial wustite; that magnetite is epitaxial, while the magnetite in Figure 17 yields a strong ring pattern.

epitaxial polycrystalline magnetite while the ring pattern of non-epitaxial polycrystalline magnetite is evident at 30 minutes (c), and stronger at 160 minutes (d). Iron does not appear in these diffraction patterns because no iron was within the region covered by the aperture used.

The appearance of iron produced by reduction using this gas mixture (at 50 torr, 373°C, 47 min) is seen in Figure 21 together with the diffraction pattern identifying iron. The faceted nature of this structure should be noted; many edges are parallel to the direction indicated by the arrow.

CONCLUDING REMARKS

On reducing magnetite with pure hydrogen, under the conditions of this investigation, incubation periods were observed. During these incubation periods no iron was evident but faceted pits formed and grew on the magnetite surface. Nucleation of iron typically occurred near these pits which were then engulfed by the advancing porous iron phase. Iron formed in the early stages of reduction was epitaxial with the host magnetite but this orientation is disrupted as reaction continues. Reduction temperature has an effect on the morphology of the iron produced and fissures were found within the iron in many instances. When using pure hydrogen the porous iron nuclei grew isotropically. With hydrogen/argon gas mixtures, reduction proceeded much more slowly. In the early stages of reduction faceted pits containing iron were formed while later these pits appeared to extend along dislocations.

Wustite was found to undergo slow changes when exposed under vacuum to the temperatures employed in this investigation. The change is thought to be disproportionation to magnetite and iron. On reduction with hydrogen, iron

was formed with a morphology similar to that produced by hydrogen reduction of magnetite; neither an incubation period nor faceted pits were observed. Polycrystalline magnetite was found after some reaction and it is conjectured that disproportionation both accompanies reduction and is promoted by it. Disproportionation was more evident on reduction using hydrogen/argon mixtures; as in the case of hematite and magnetite, reduction with this gas mixture was remarkably slow, and (as in the case of magnetite) anisotropic.

This two part paper has used a relatively new experimental technique to examine microstructural aspects of the reduction of iron oxides by hydrogen. The investigation has been a restricted one, examining only single crystals at moderate temperatures and with little variation in gas pressure/composition. Nevertheless the results to date suggest that the technique is a powerful one that can add to our understanding of this technologically important group of reactions.

ACKNOWLEDGMENT

This work was supported by the Director, Office of Energy Research, Office of Basic Energy Sciences, Materials Sciences Division of the U.S. Department of Energy under Contract Number DE-AC03-76SF00098.

REFERENCES

1. E. T. Turkdogan, R. G. Olsson and J. V. Winters: Metall. Trans. 2(1971), p.3189.
2. W. Pluschkell and B. V. S. Sarma: Arch. Eisenhuttenwes. 45(1974), p.23.

FIGURE CAPTIONS

Fig. 1 Sequence electron micrographs showing the reduction of magnetite. The specimen was reduced by 2 torr in pure hydrogen at 300°C. Numbers inserted are the reduction time in seconds.

Fig. 2 Overview of the region of Figure 1 before (a) and after (b) reduction. The arrows indicate the thinner region of the specimen, which might be the favored sites for nucleation of the iron phase.

Fig. 3 Electron micrographs showing the development of faceted pits on partially reduced magnetite. The specimen was brought back to room temperature after the first stage reduction by 2 torr pure hydrogen at 300°C for 14 min, then was reduced again at the same temperature for 2 (a) and 3 (b) minutes.

Fig. 4 Bright and dark field images of faceted pits showing a close relationship between the pits and the parent magnetite matrix.

Fig. 5 Bright and dark field images of retained pits.

Fig. 6 Bright and dark field images of the magnetite specimen after reduction with 1 torr hydrogen at 330°C for 21 minutes.

Fig. 7 (a) Bright field image of porous iron formed in reducing magnetite with 10 torr pure hydrogen at 400°C for 1 min. (c) and (d) are corresponding dark field images from A and B reflections indicated in the electron diffraction pattern (b). (c) reveals iron clusters and (d) reveals residual magnetite.

Fig. 8 (a) Bright and (b) dark field images of porous iron formed by reducing a magnetite specimen in 20 torr pure hydrogen at 350°C for 10 seconds. The iron nuclei were sintered by heating the partially reduced specimen up to 500 °C for 2 min in vacuum and their bright and dark

field images are shown in (c) and (d), respectively. The same specimen was further reduced at lower temperature, i.e. 305°C, for 2 min with 20 torr pure hydrogen and its bright field image (d) reveals that the sizes of iron nuclei and pores are larger than the sizes in (a).

Fig. 9 (a) Typical star shaped pores in product iron. (b) Pores formed in one iron clusters only when two iron nuclei coalesced. The magnetite specimen was reduced by 2 torr hydrogen at 300°C for 13 min and 5 sec.

Fig. 10 Reduction occurs in several preferential directions with a low reducing potential gas mixtures, 10% H_2/90% Ar. The morphology shown in t=0 is an iron cluster which was obtained by prior reduction in a pure hydrogen atmosphere. The partially reduced magnetite then was exposed to 10 torr 10% H_2/90% Ar at 350°C. The morphology of the iron cluster changes during reaction. The number inserted is the time in minutes.

Fig. 11 Schematic diagram illustrating the development of an iron cluster under low reducing potential.

Fig. 12 A crack provides the reaction site for reduction under low reducing potential. The magnetite specimen was reduced at 514°C using 50 torr 10% H_2/90% Ar. The numbers inserted are the reducing time in minutes.

Fig. 13 Dislocation loops provide the interaction sites for reduction under low reducing potential. The magnetite specimen was reduced at 350°C for 3 hr and 12 min using 10 torr 10% H_2/90% Ar.

Fig. 14 Disproportionation of wustite at 500°C in vacuum. The numbers inserted are the duration time in minutes.

Fig. 15 (a) Rectangular magnetite nuclei occurred after heating the wustite in vacuum at 500°C for 40 minutes. (b) The magnetie nuclei grew

preferentially in one direction. The electron micrograph was taken after 56 min. (c) The magnetite nuclei were dissolving back into the matrix after the temperature was brought up to 600°C for 36 minutes.

Fig. 16 Sequence electron micrographs showing the reduction of wustite using 10 torr pure hydrogen at 350°C for the time inserted in minutes. Morphological change is similar to that of magnetite reduction, however, there is no incubation period or faceted surface observed.

Fig. 17 Typical diffraction pattern taken from iron nuclei showing that only iron and magnetite coexist.

Fig. 18 Electron micrographs of wustite reduction following Figure 52. Disproportionation and reduction occurred simultaneously.

Fig. 19 Schematic illustrating the formation on pit. Oxygen moves outward to build a lump of magnetite rich region and iron is left behind in the center of the pit.

Fig. 20 Electron diffraction patterns showing the transformation of single crystal wustite --> epitaxial crystal magnetite --> polycrystalline magnetite. The specimen was reduced using 50 torr 10% H_2/90% Ar at 514°C for 0 (A), 14 (b), 30 (c) and 160 (d) minutes, respectively.

Fig. 21 Porous iron formed in a wustite specimen after reducing at 373°C for 105 min using 5% H_2/95% Ar.

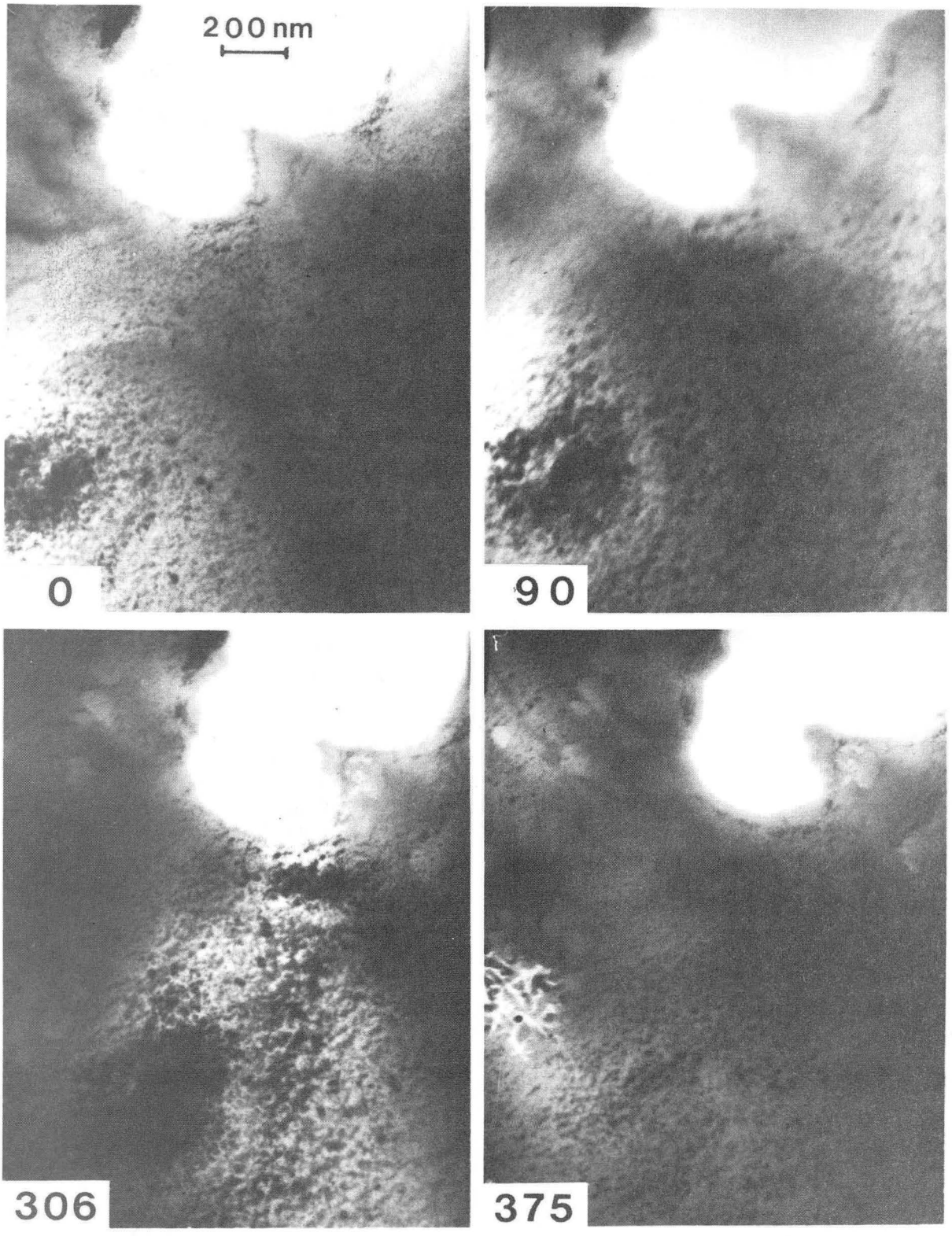

Figure 1.

XBB 840-9194

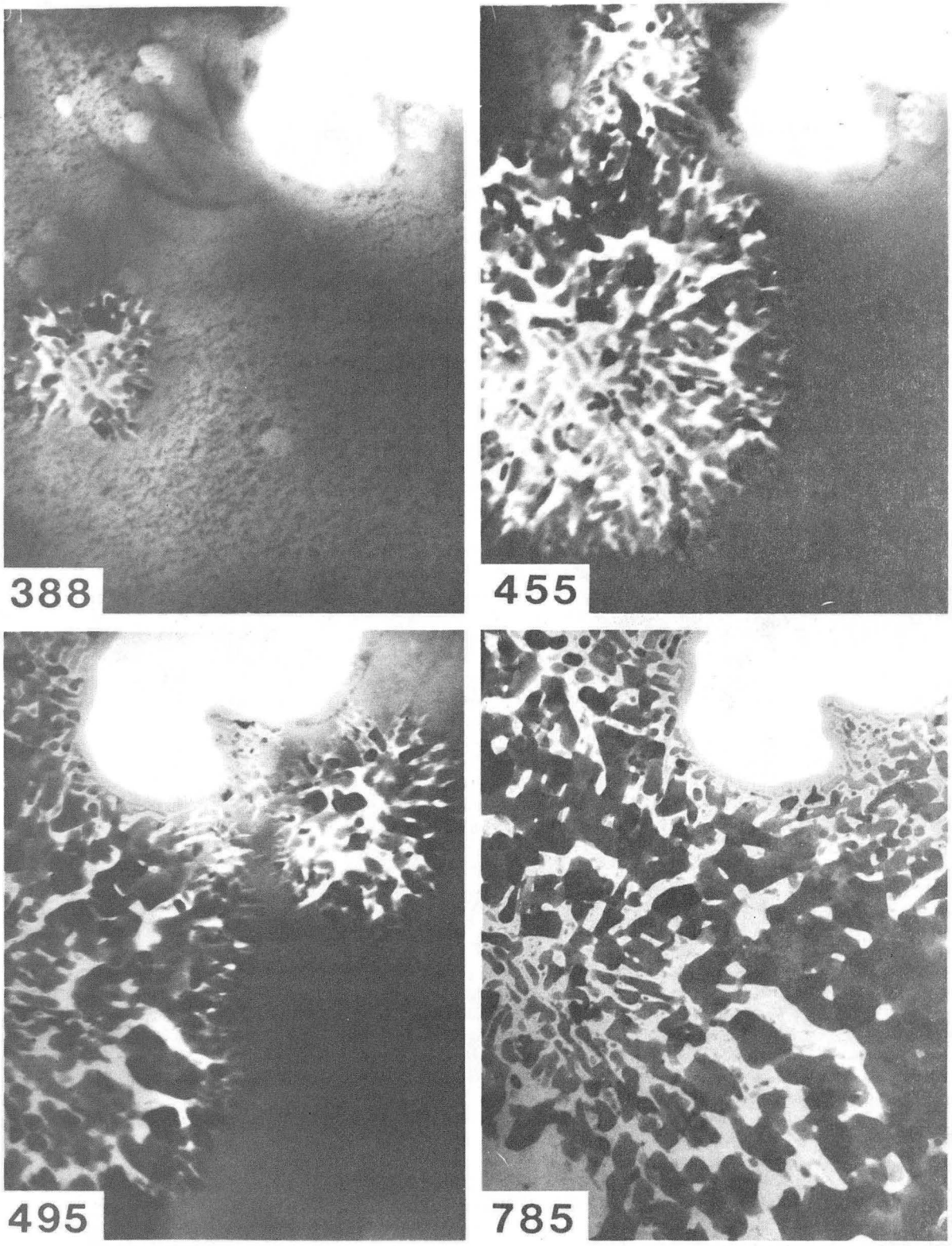

Figure 1.

XBB 840-9193

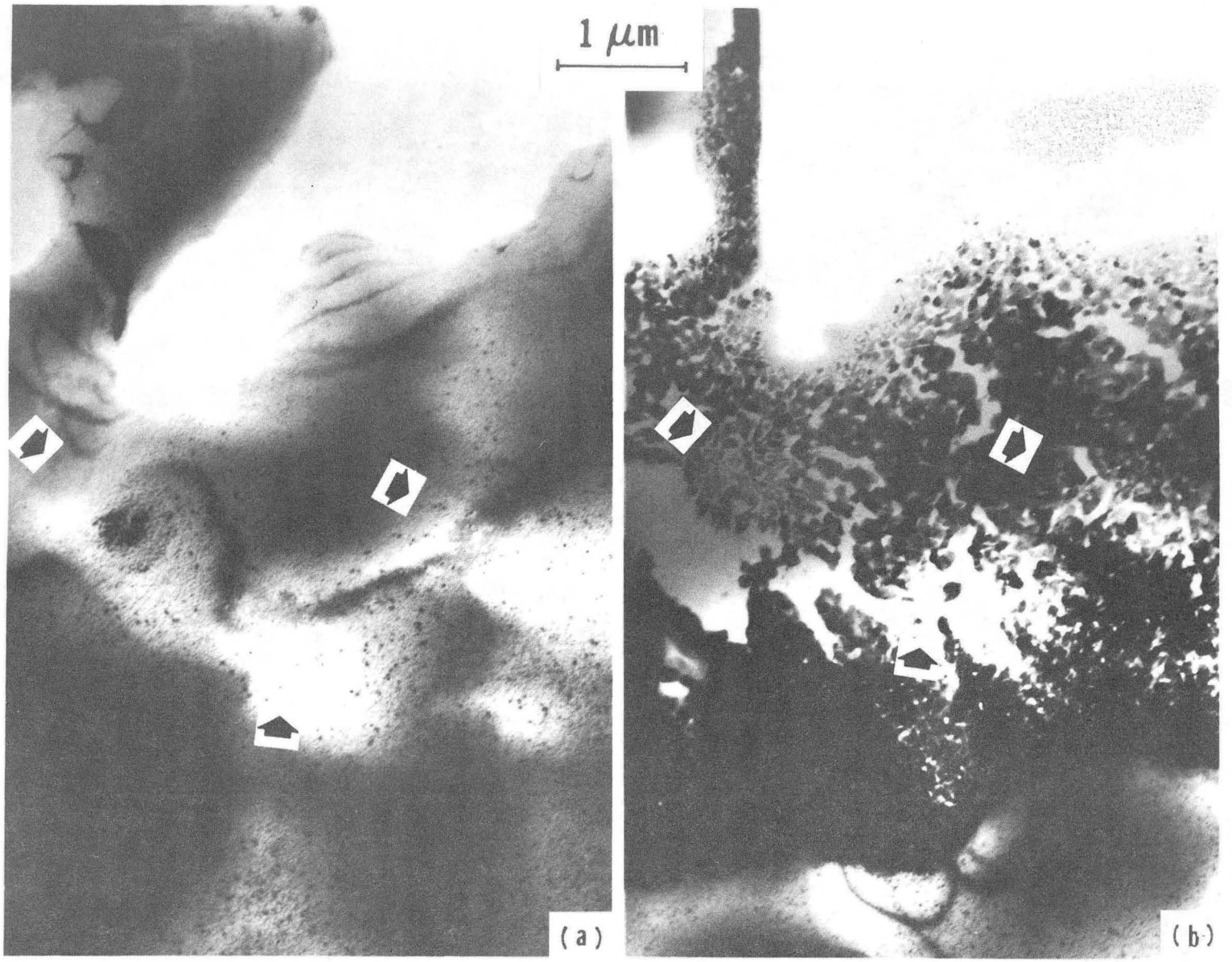

Figure 2.

XBB 840-9184

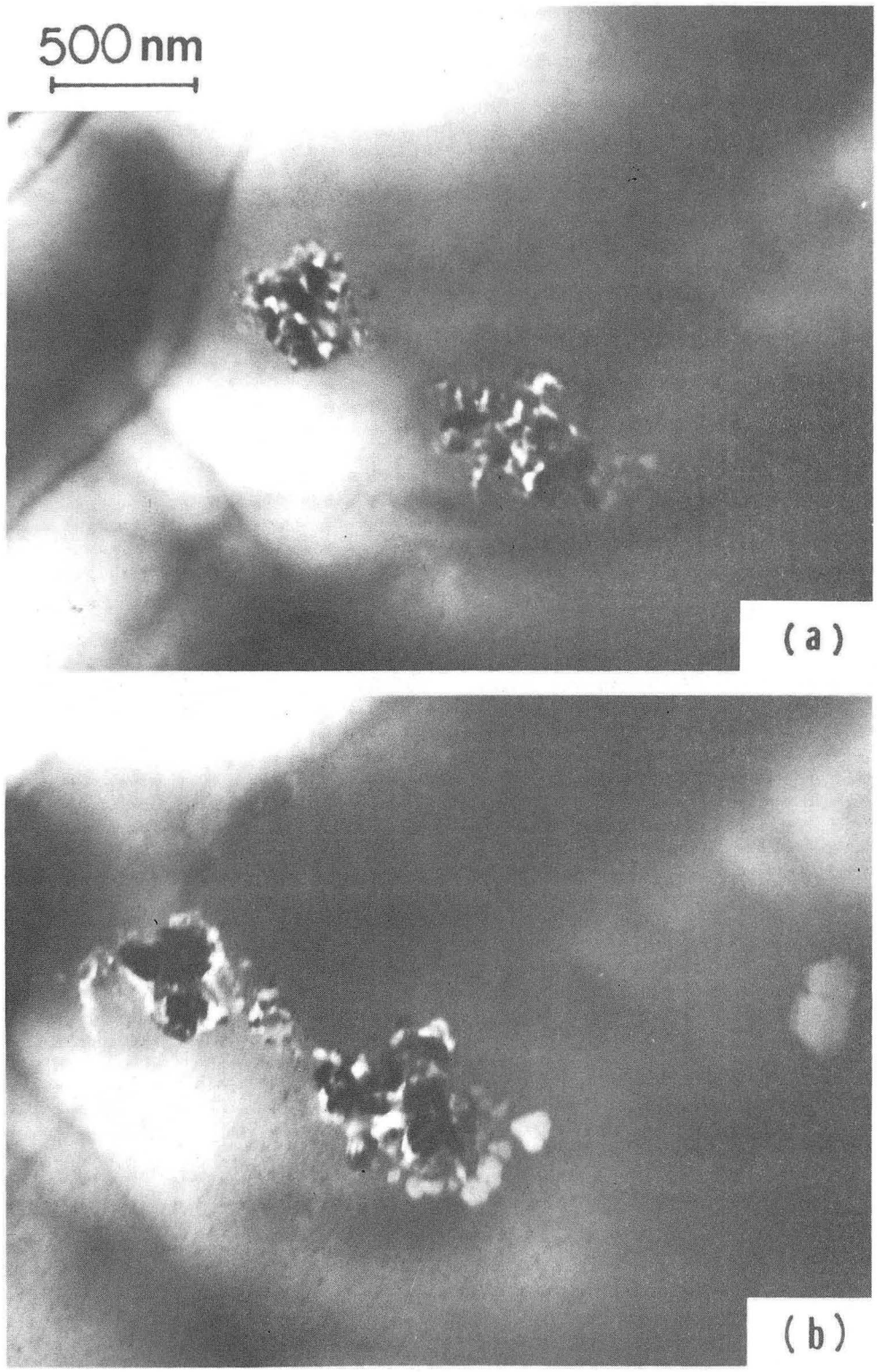

Figure 3.

XBB 840-9191

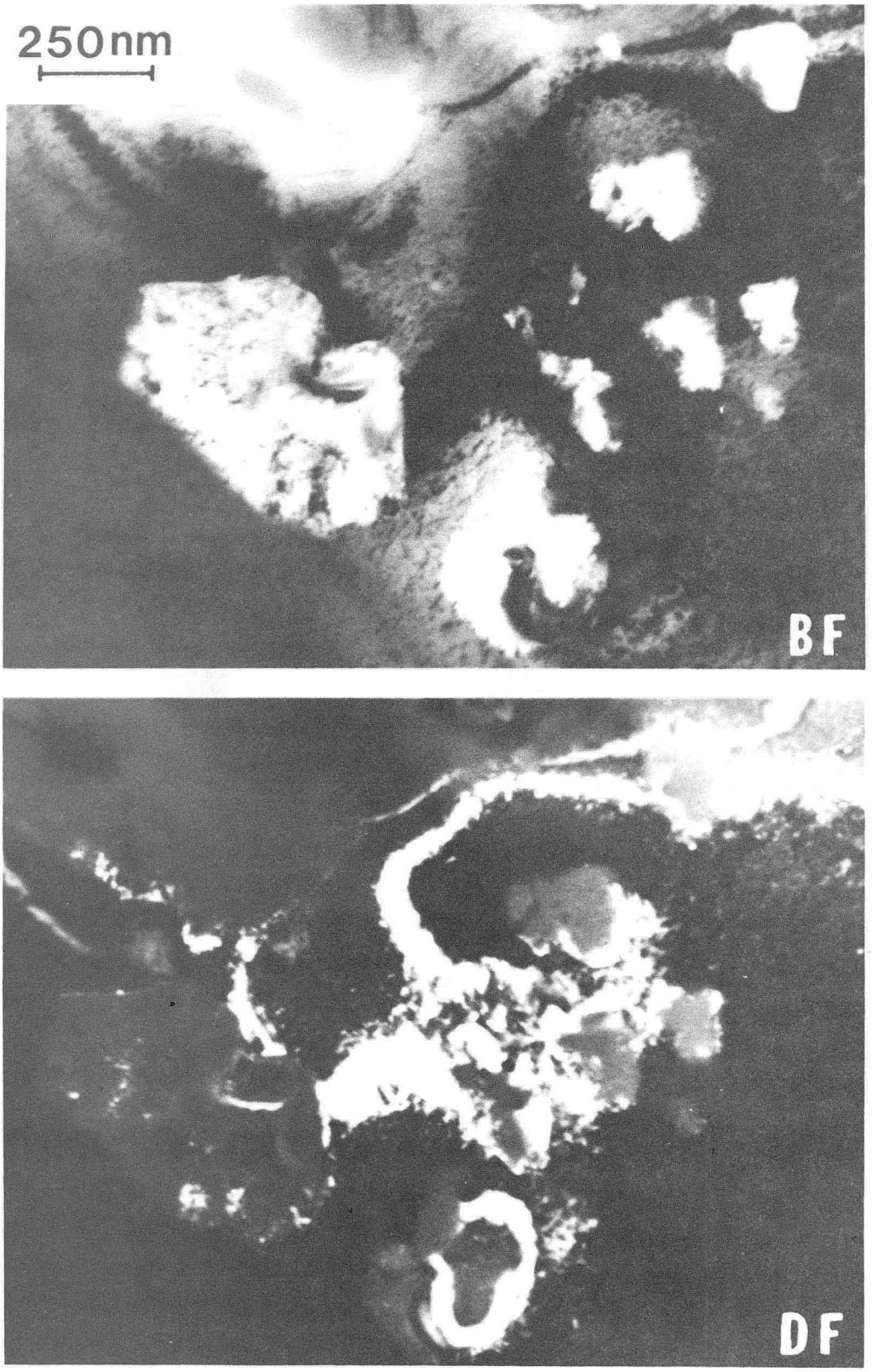

Figure 4.

XBB 840-9192

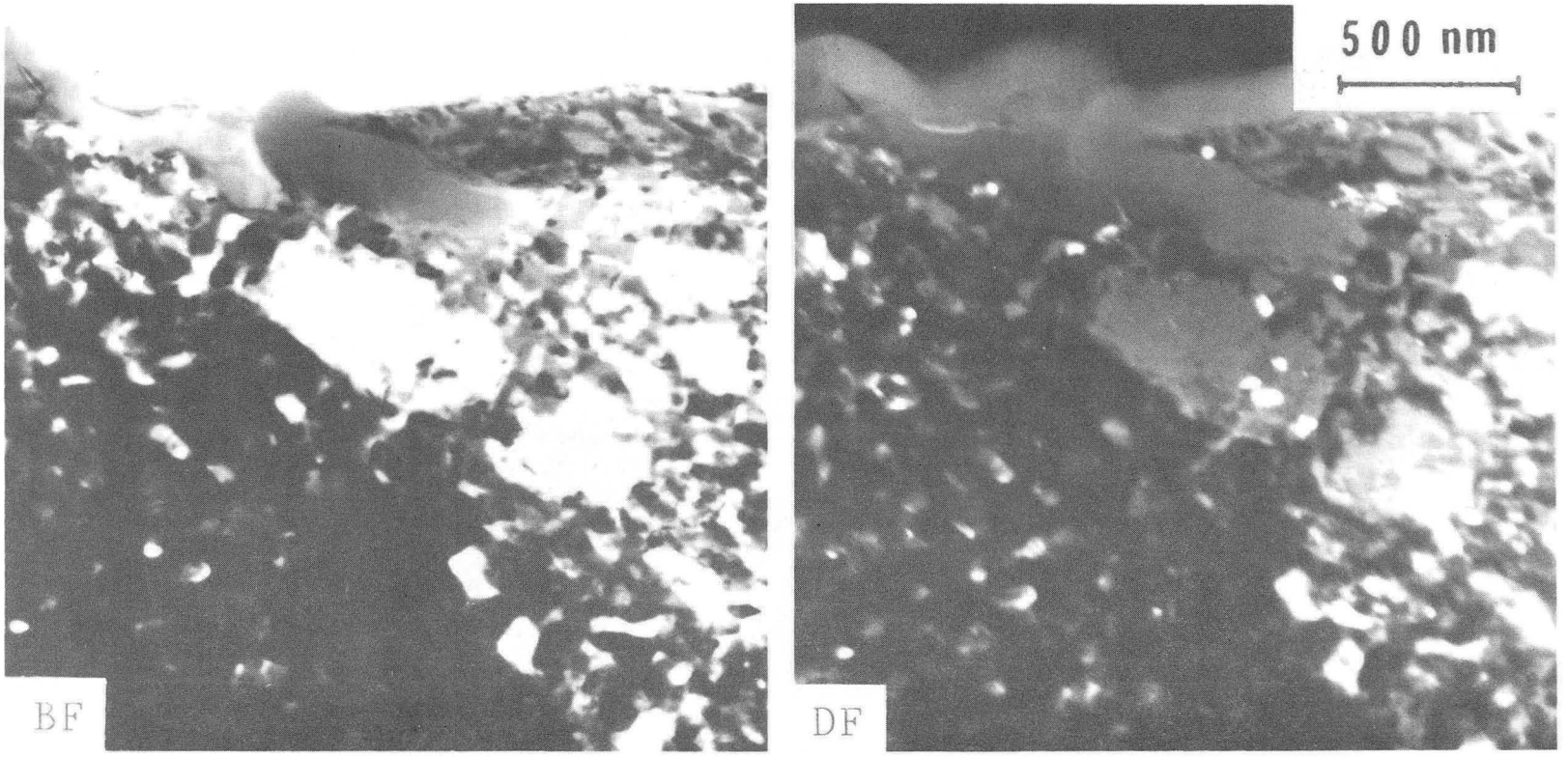

Figure 5.

XBB 840-9593

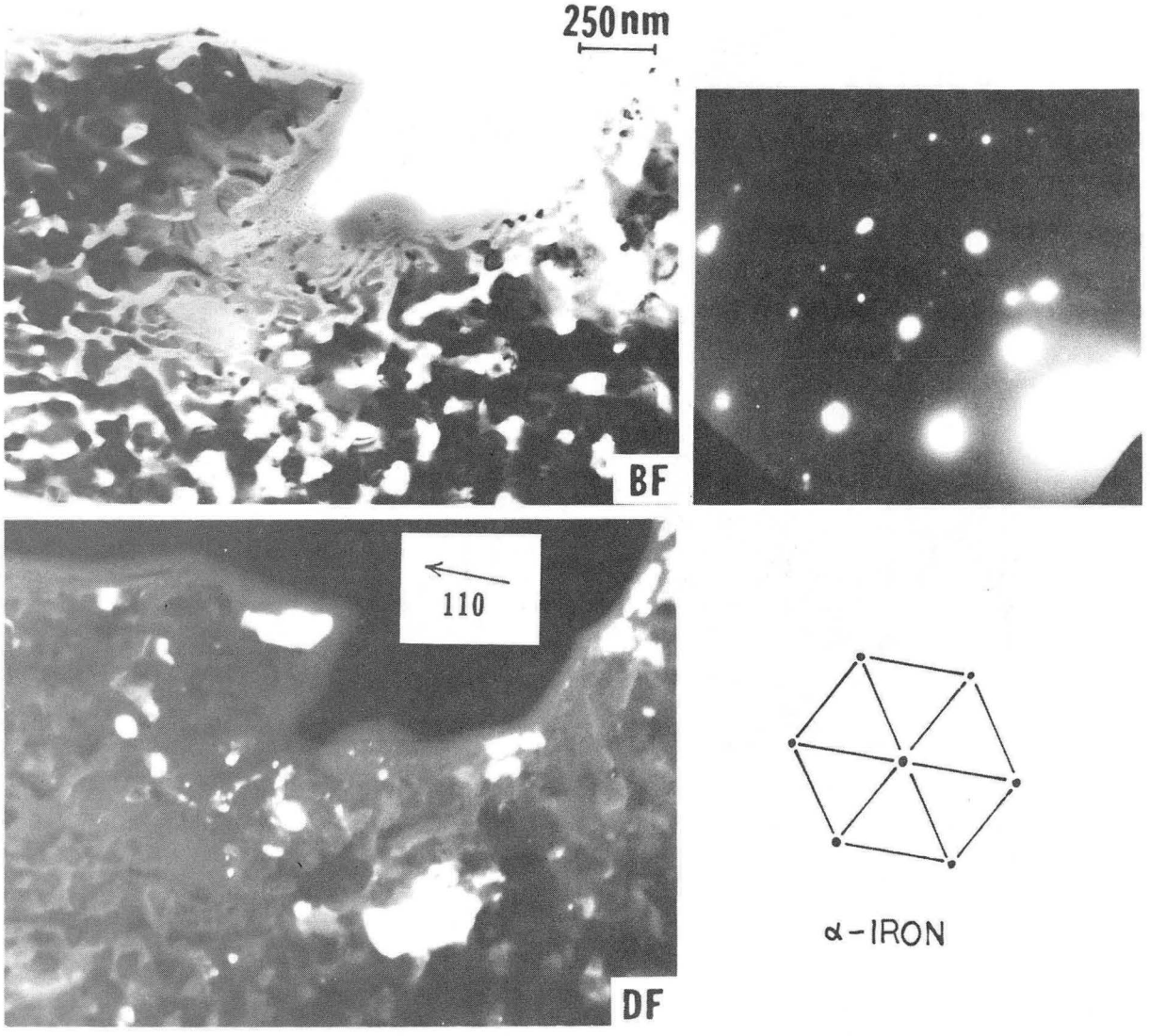

Figure 6.
XBB 840-9584

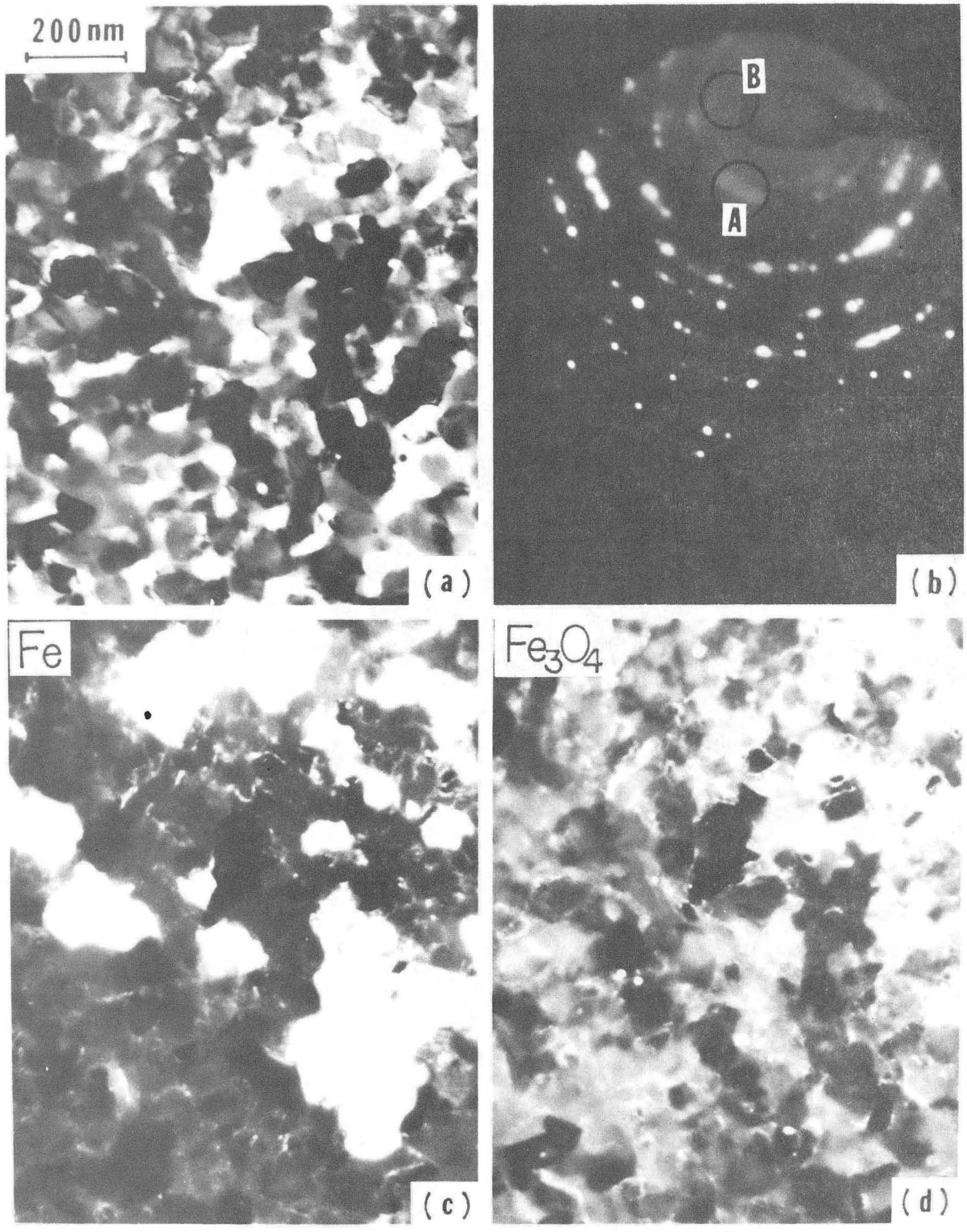

Figure 7.

XBB 840-9604

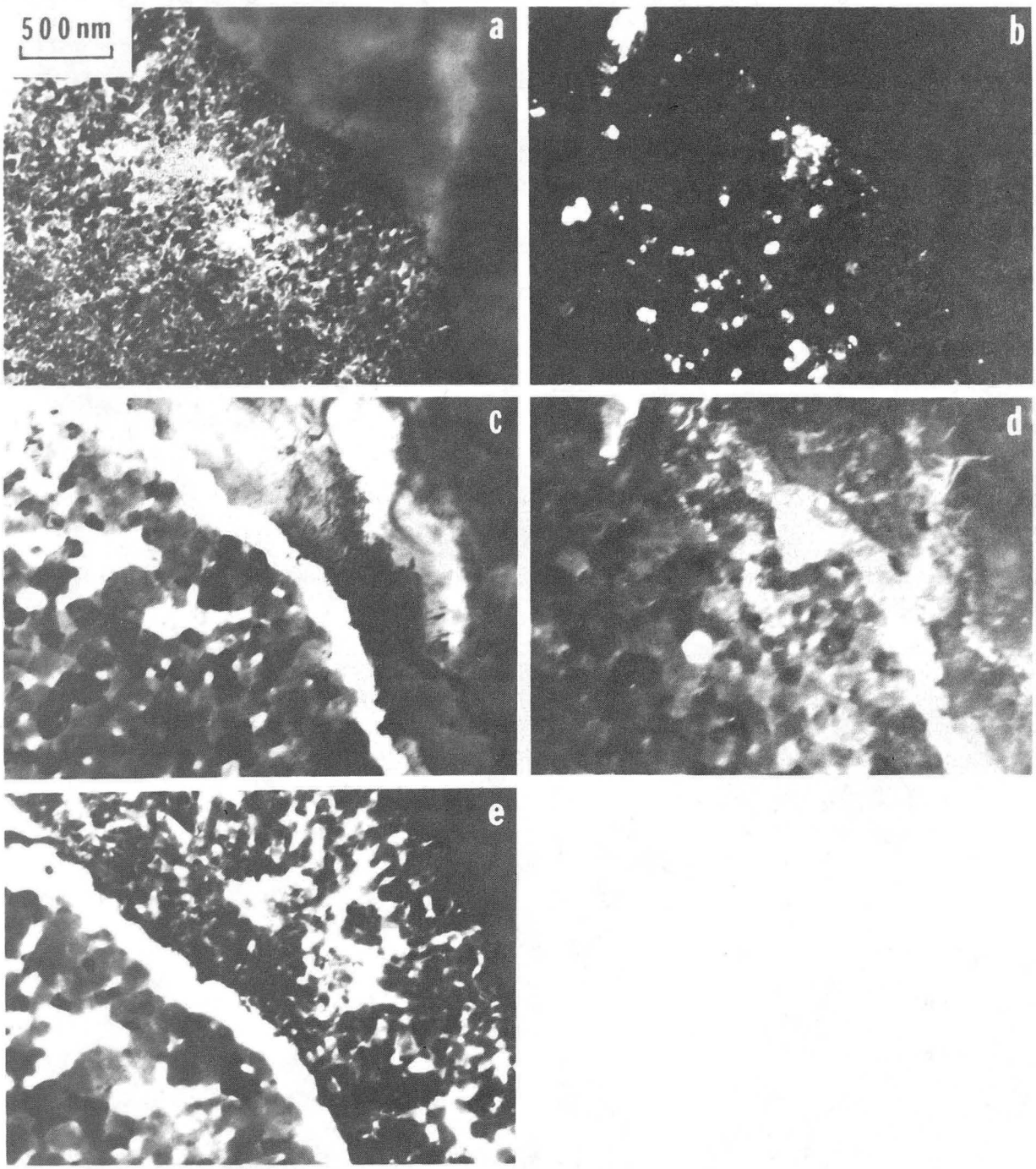
500nm
a
b
c
d
e

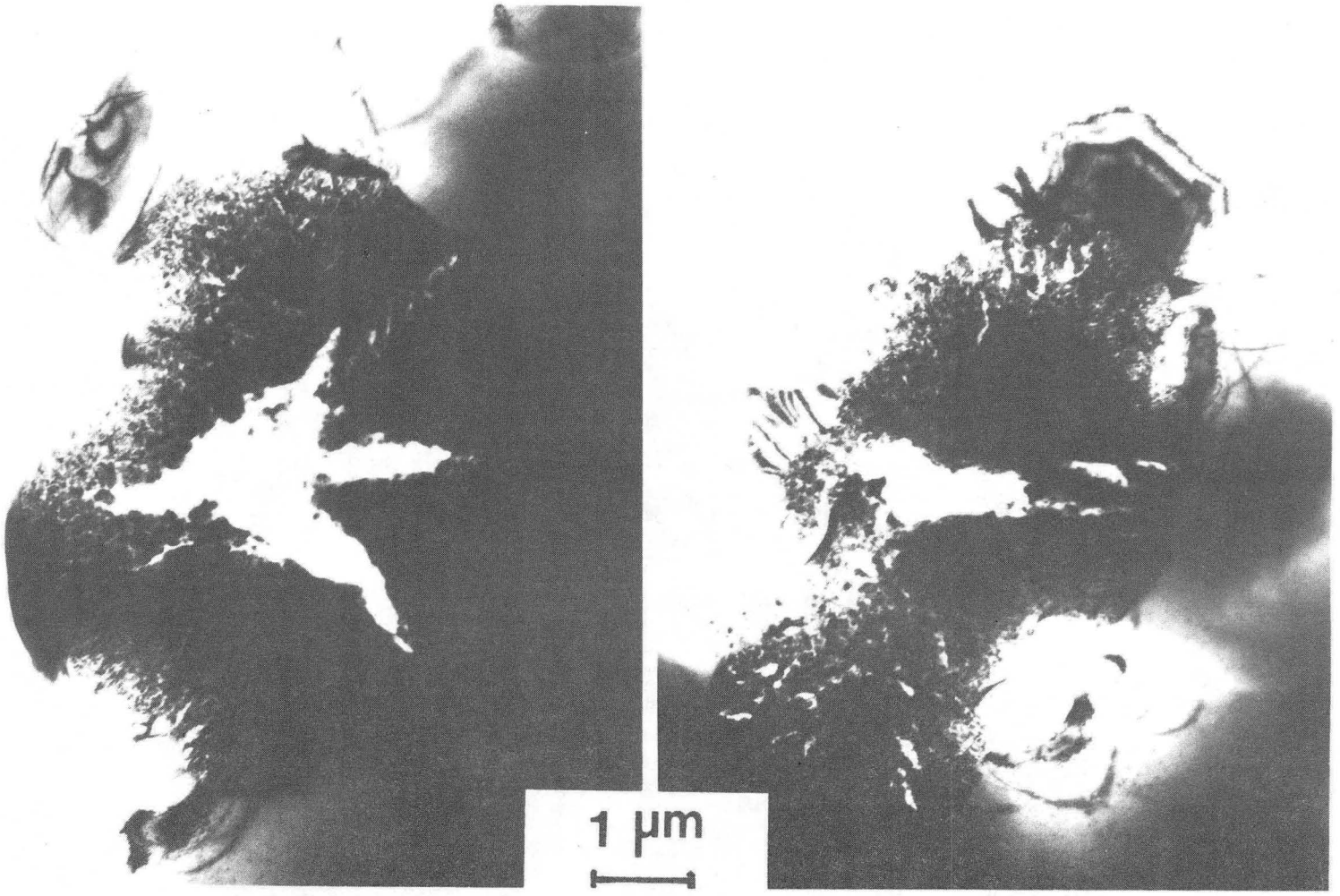

Figure 9.

XBB 840-9185

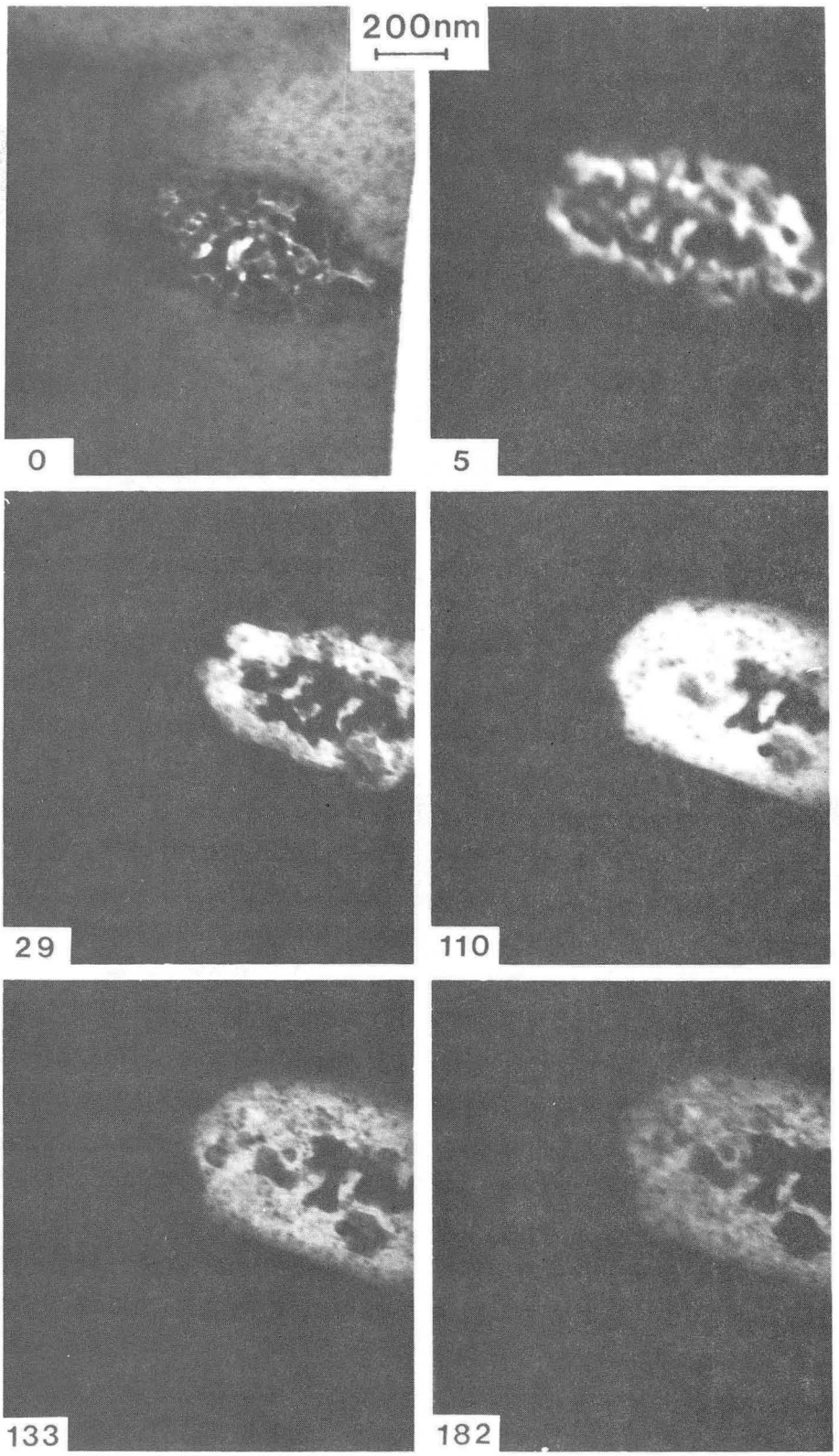

Figure 10.

XBB 840-9183

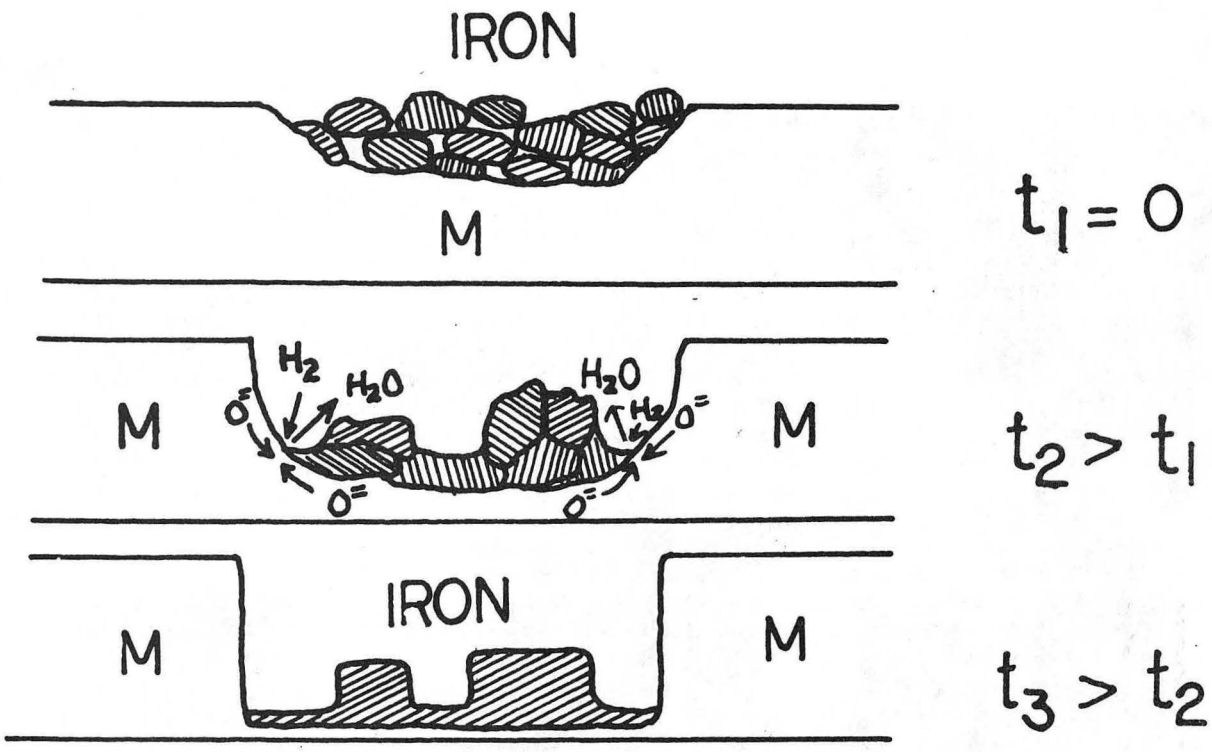

XBL 8412-5443

Figure 11.

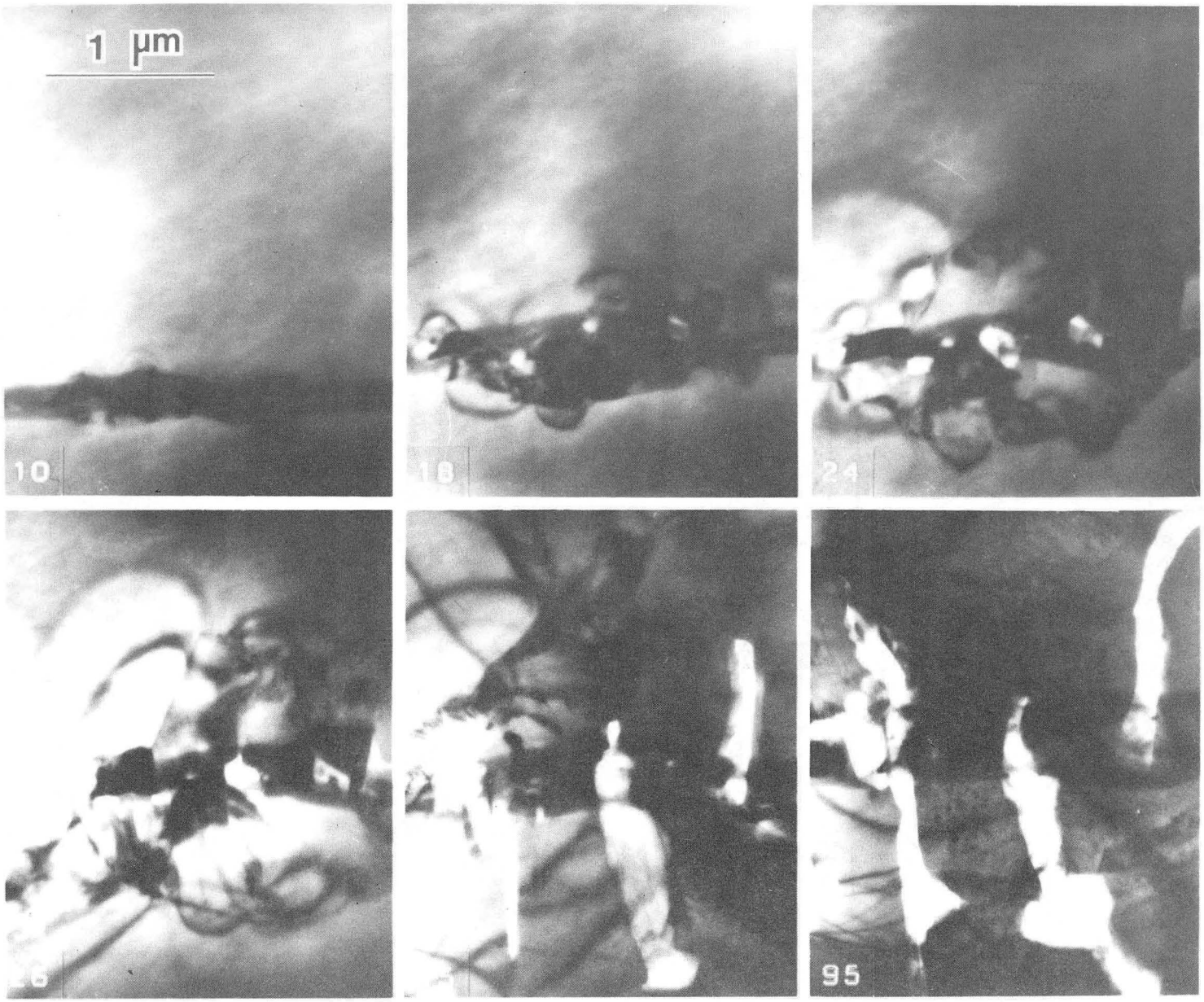

Figure 12.

XBB 830-10290

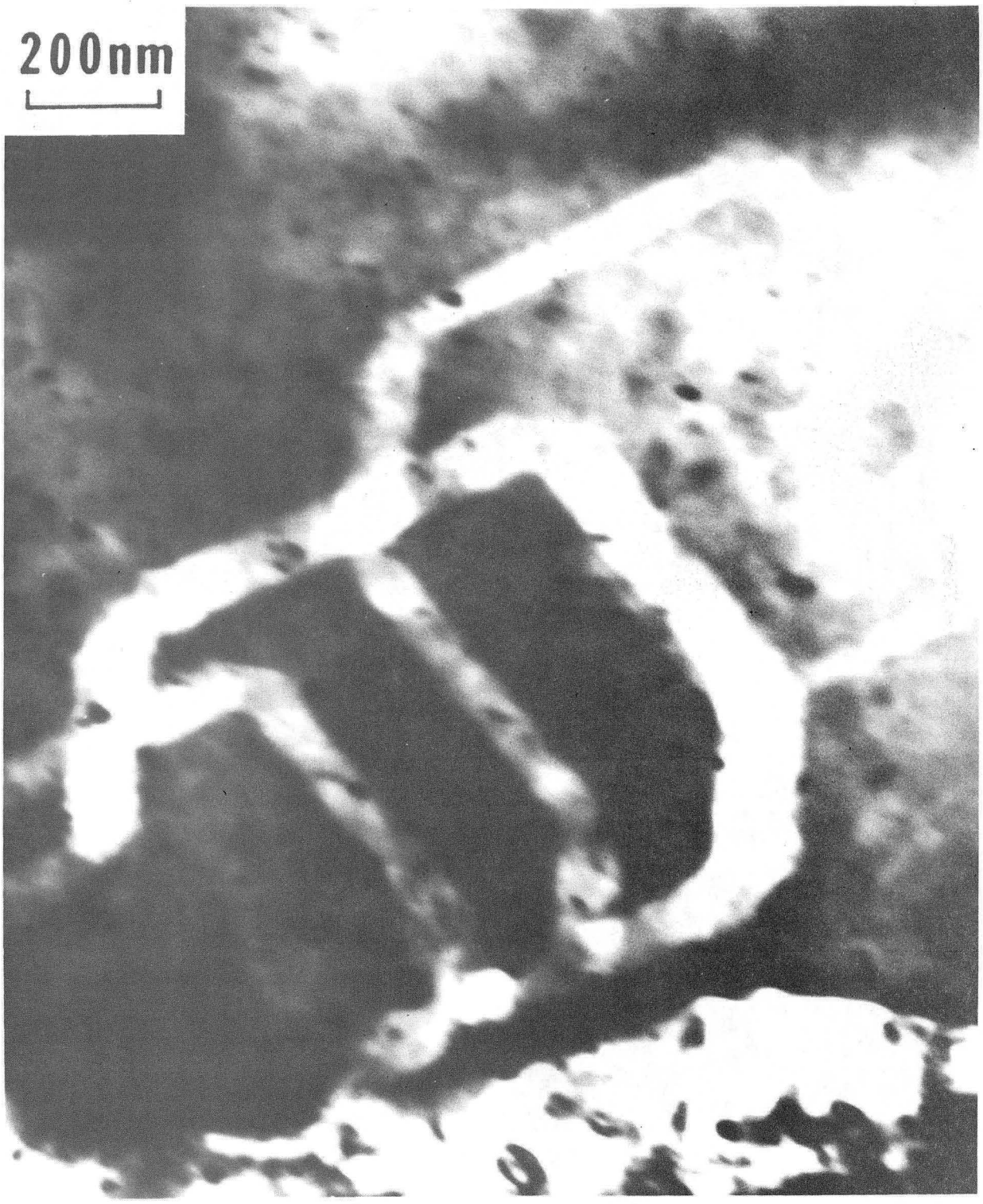

Figure 13.

XBB 840-9190

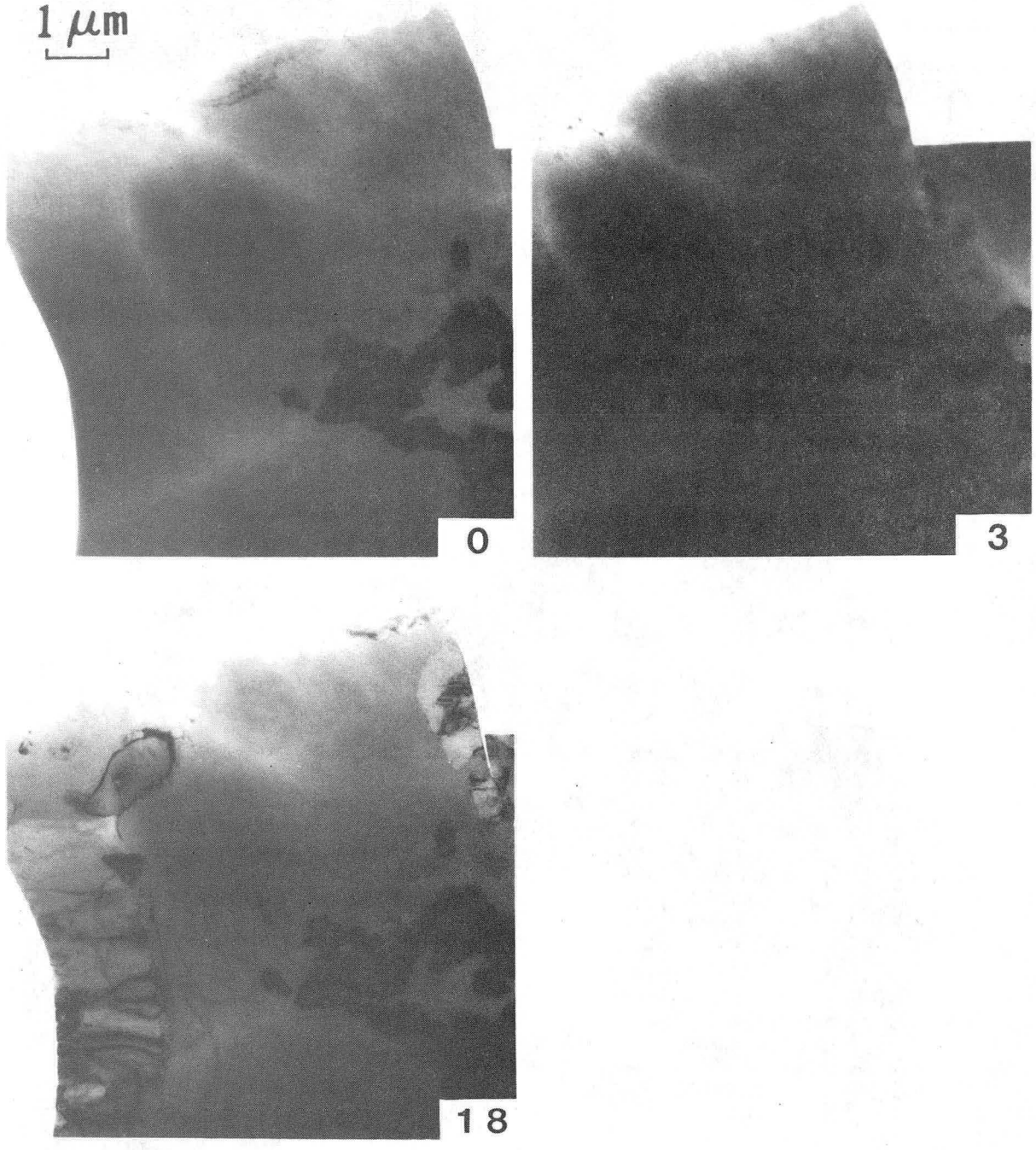

Figure 14.

XBB 840-9592

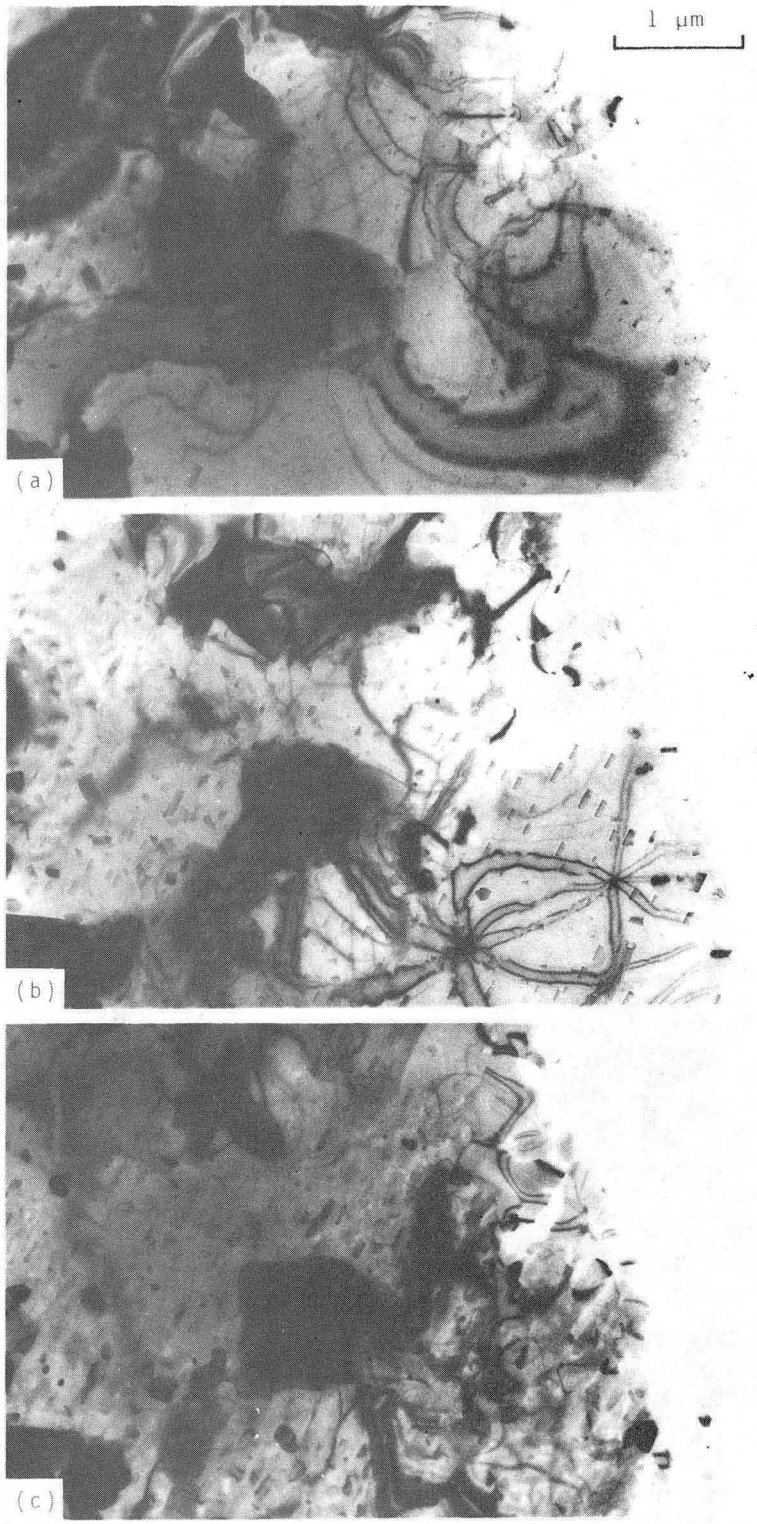

Figure 15.

XBB 840-9181

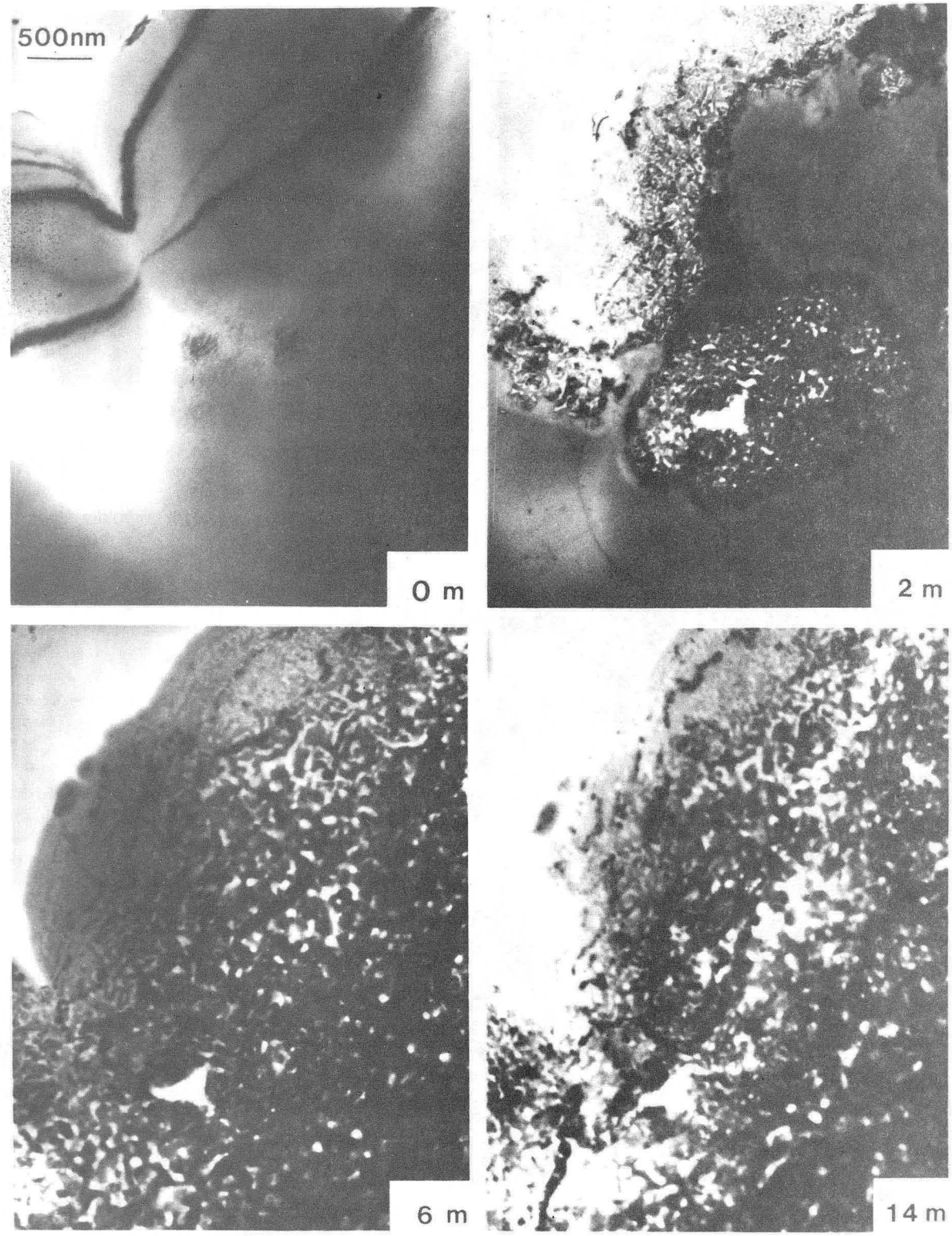

Figure 16.

XBB 840-9189

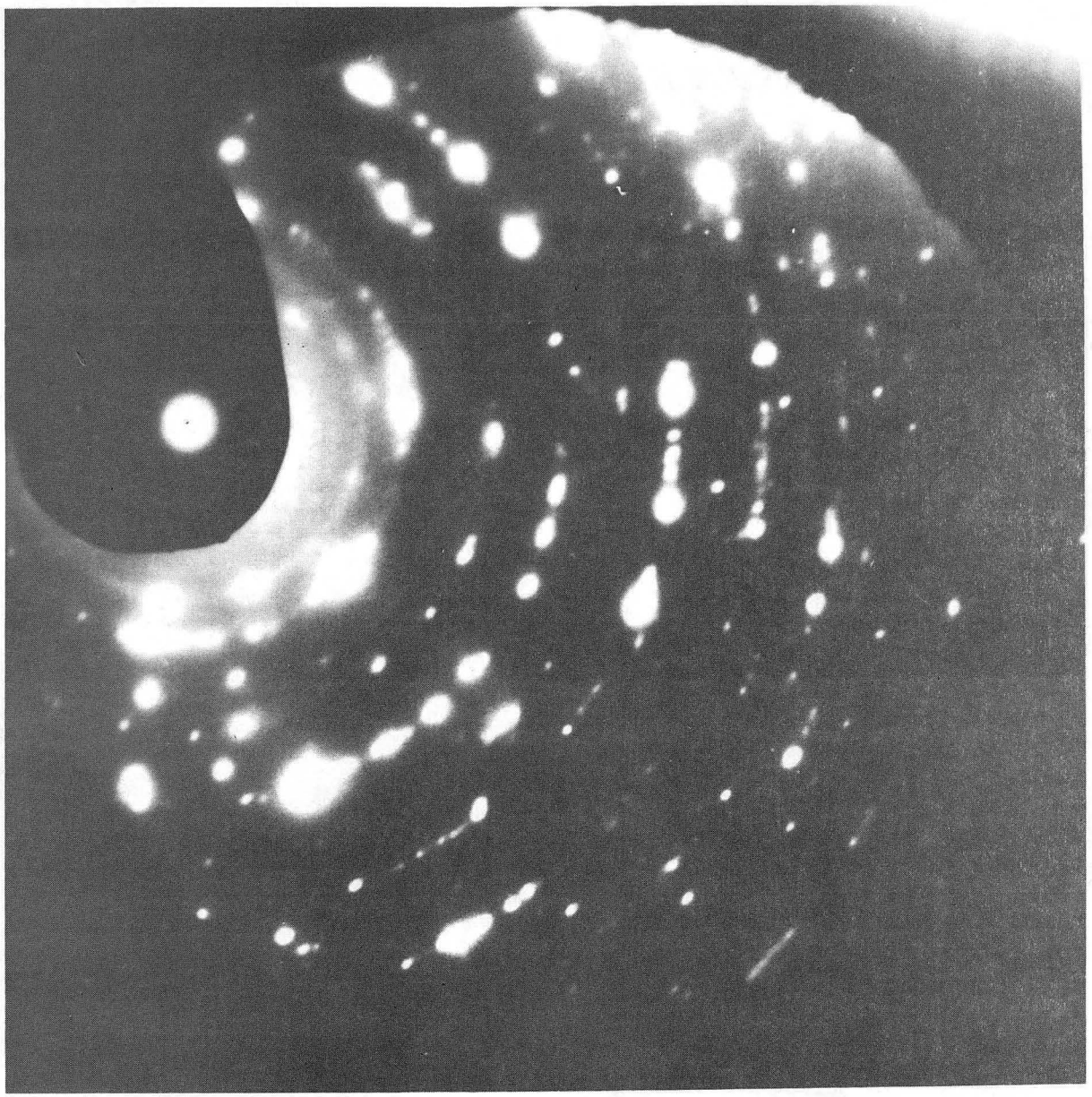

Figure 17.

XBB 840-9601

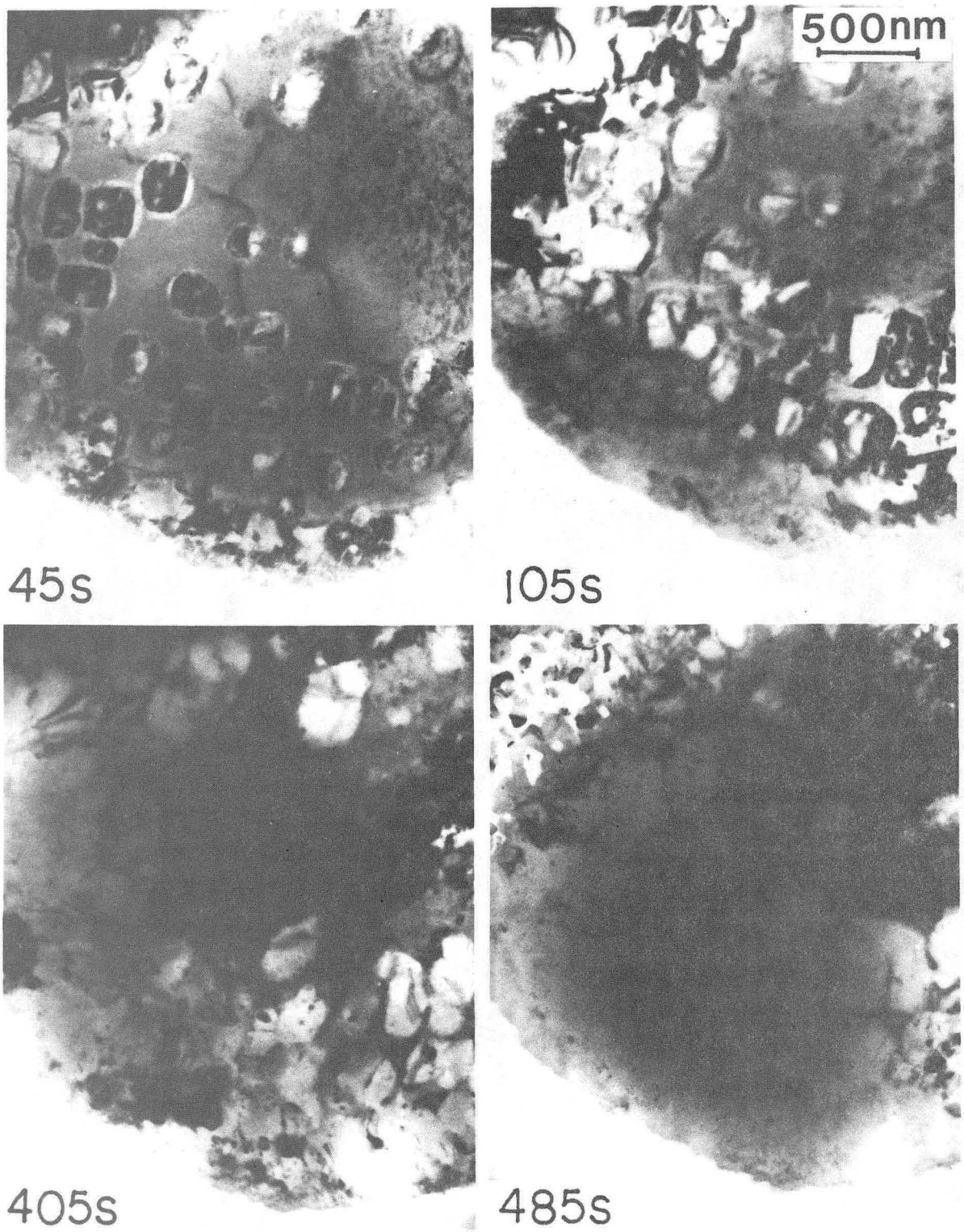

Figure 18.

XBB 840-9187

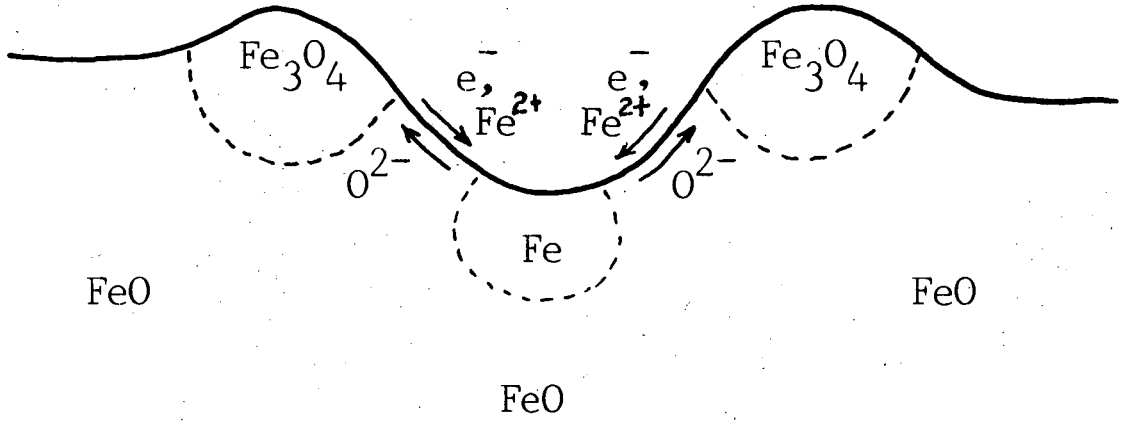

XBL 8412-5445

Figure 19.

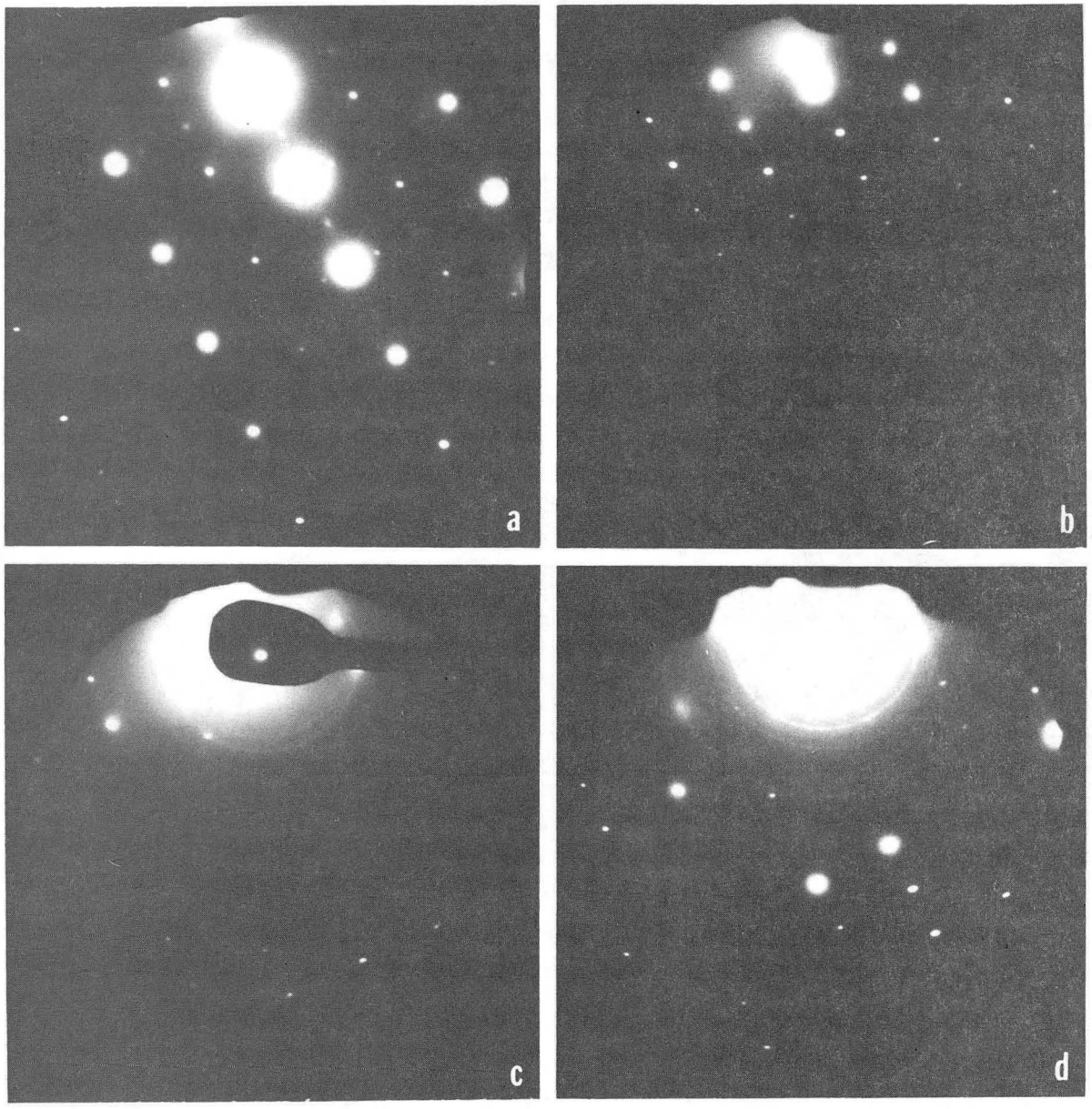

Figure 20.

XBB 840-9589

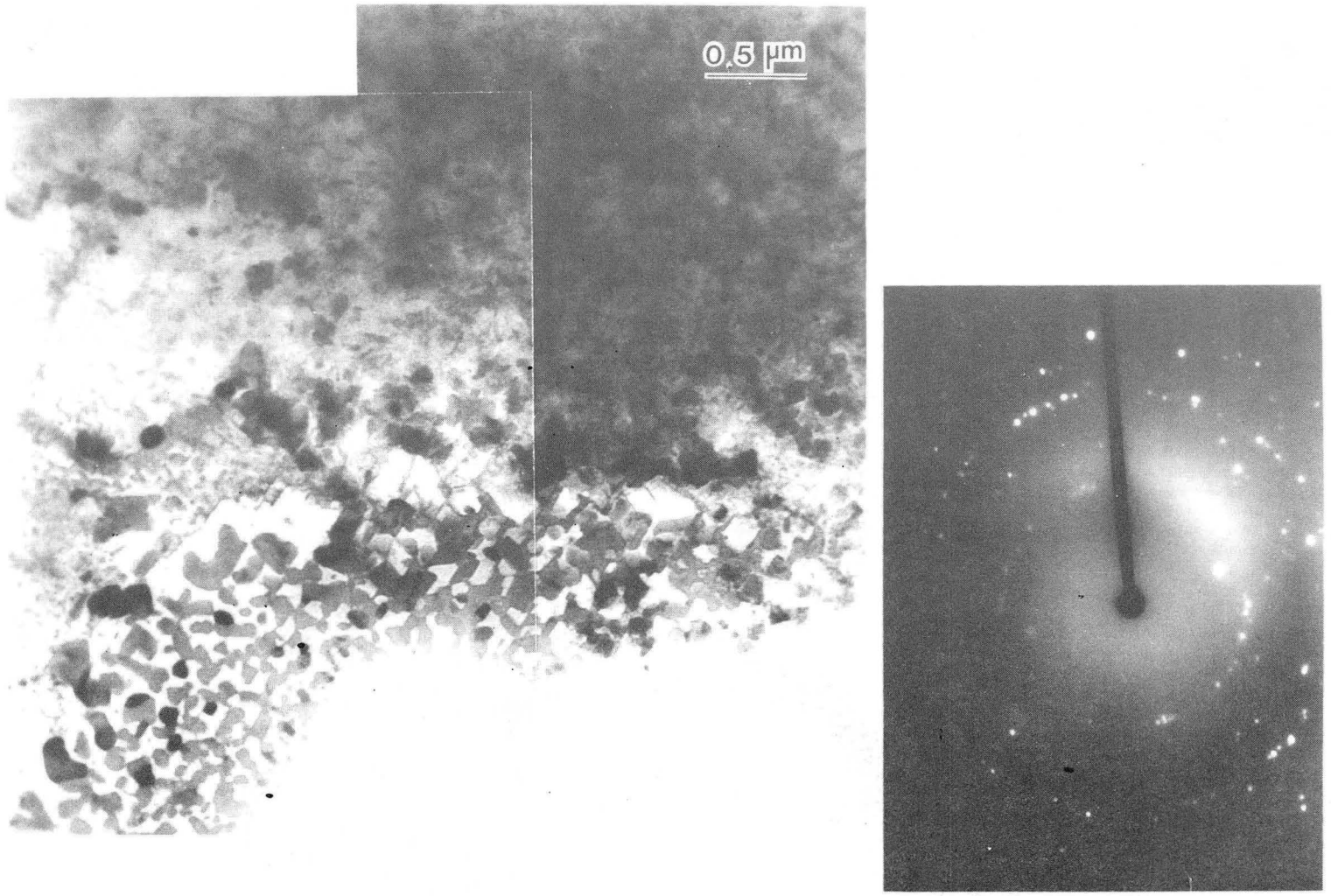

Figure 21.

XBB 830-10293

LAWRENCE BERKELEY LABORATORY
TECHNICAL INFORMATION DEPARTMENT
UNIVERSITY OF CALIFORNIA
BERKELEY, CALIFORNIA 94720